APPARENT TELEPORTATION OF INDISTINGUISHABLE PARTICLES

Marek Gazdzicki [a,†], Daniel Kikola [b], Ivan Pidhurskyi [a]
Leonardo Tinti [a]

[a]Jan Kochanowski University in Kielce, Kielce, Poland
[b]Warsaw University of Technology, Warsaw, Poland

Received 8 March 2026, accepted 18 March 2026, published online 28 May 2026

Teleportation, introduced in science fiction literature, is an instantaneous change of the position of a macroscopic object. Two teleportation-like phenomena have been predicted by quantum mechanics: quantum teleportation and, more recently, quantum particle teleportation. Here, we introduce the third teleportation-like phenomenon — apparent teleportation. It seems to be a natural consequence of the Standard Model's indistinguishable elementary particles and antiparticles. We illustrate the idea within a 1+1D toy model of particle–antiparticle creation and space-time evolution obeying transport locality. Furthermore, we propose a novel method to observe apparent teleportation driven by strong interactions through measurements of correlations between the momenta of charm and anticharm hadrons in nuclear collisions. Observing the apparent teleportation would uncover the basic transport properties of indistinguishable particles.

DOI:10.5506/APhysPolB.57.6-A17

1. Introduction

Teleportation [1] is rooted in science fiction. It describes the ability of macroscopic objects, such as humans, to reappear at a distant location without traversing space. Thus, the speed of light does not limit the possibility of changing our spatial location. Needless to say, this also concerns signals. Details depend on the science fiction setup.

Quantum teleportation [2] is the standard quantum physics phenomenon — transferring quantum-state properties over arbitrarily large distances in no time. In quantum teleportation, conditional probabilities of measurement outcomes reappear at a distant location using the entanglement of two particles. There is neither a super-luminal transfer of conserved quantities nor super-luminal signalling. Quantum teleportation is measured in numerous experiments [3–6].

† Corresponding author: marek.gazdzicki@cern.ch

Quantum particle teleportation [7] is an instantaneous transfer of a single particle over a large distance predicted by standard quantum mechanics. The phenomenon appears for particles in a potential. It is induced by frequently monitoring if the particle is at rest (a peculiar quantum Zeno dynamics [8–10]). Quantum particle teleportation exhibits the properties of "science fiction" teleportation, allowing for the reappearance of conserved quantities and signalling. It was predicted in 2023 and has yet to be experimentally tested.

Apparent teleportation (AT) is a concept introduced here. It is defined as the time evolution of a system of indistinguishable particles that cannot be mimicked by classical distinguishable particles moving with luminal or subluminal velocities. Of course, when referring to distinguishable particles mimicking indistinguishable ones, we assume the observer is blind to particle labels. AT seemingly requires superluminal velocities of particles. This illusion arises from the fact that particle trajectories and velocities are defined for distinguishable particles but are undefined for indistinguishable ones.

2. Results

Elementary particles and antiparticles of the Standard Model are indistinguishable bosons and fermions. Objects composed of many indistinguishable elementary particles and antiparticles are close to unique and thus can be approximately treated as distinguishable ones[1]. Classical physics is rooted in our daily experience within the world of macroscopic, distinguishable objects, including humans. In particular, it is well established that they can move only with velocities smaller than the speed of light. However, applying the time-evolution limits of distinguishable objects to indistinguishable particles and antiparticles imposes a human-centred experience on a fundamentally different world. The inadequacy is obvious if these limits are given in quantities that are undefined for indistinguishable particles and antiparticles, such as particle velocity. In this sense, apparent teleportation is the natural property of models postulating the indistinguishability of elementary particles and antiparticles.

In what follows, we illustrate the concept of apparent teleportation in a toy model of particle–antiparticle creation, annihilation, and transport. Importantly, we propose a novel method that allows for observing the apparent teleportation in collisions of two nuclei, if it exists.

[1] An internally consistent model covering distinguishable and indistinguishable particles and antiparticles has to give identical predictions for a single particle or antiparticle in the system when treating it as distinguishable and indistinguishable.

2.1. Toy model of apparent teleportation

Cell Model is a dynamical model based on the 1+1D discrete-time Markov chain framework [11, 12]. Space is assumed to be a vector of V discrete cells $(v_1, v_2, \ldots, v_V)$ arranged in a ring. At the given time t, the system microstate is fully defined by a cell distribution of particles and antiparticles. The system's evolution in time is assumed to be discrete, and the time steps are numbered by t. During evolution, transitions occur between microstates. The transition probability from a microstate X at t to a microstate Y at $t+1$ depends only on the microstate X — the basic assumption of Markov chains.

To illustrate the concept of apparent teleportation, we consider three types of reactions changing the system's microstates:

— particle–antiparticle creation in a single cell,

— particle–antiparticle annihilation in a single cell and,

— redistribution of particles and antiparticles between cells.

The first two reactions change the number of particles and antiparticles, whereas the third only changes the distribution of (anti)particles in cells. The difference between the particle and antiparticle number of a given type is conserved in the whole system. This is the only conservation law that applies to the system.

To summarise, the distributions of particles and antiparticles in cells generally differ across time steps. This can be due to particle–antiparticle creation–annihilation reactions and particle and antiparticle redistribution. We now postulate that only changes that obey transport locality are allowed during the redistribution. For distinguishable particles, the transport-locality requirement reduces to a requirement of each particle moving by no more than Δ cells. In physics, this corresponds to particle velocities, which are limited by the speed of light in a vacuum.

For indistinguishable particles, the particles' trajectories and thus velocities are undefined. Thus, the transport-locality condition for distinguishable particles does not apply to indistinguishable ones. The condition for indistinguishable particles and antiparticles is unknown, and experiments are needed to uncover it.

Here, we assume that the transport-locality condition introduced for conserved particle number in Ref. [12] (see below) is valid separately for redistributions of indistinguishable particles and antiparticles. It implies the following. During a single time step, the particle (antiparticle) number in any interval of cells cannot be transported beyond an interval by Δ cells longer on the left and right. Moreover, it cannot be squeezed into an interval

by Δ cells shorter on the left and right. The condition means that only those redistributions of particles (antiparticles) that can be mimicked by distinguishable particles (antiparticles) are possible. The condition is given by two transport-locality inequalities [12]

$$\sum_{j=i}^{i+k} n_j^X \leq \sum_{l=i-\Delta}^{i+k+\Delta} n_l^Y ,$$
$$\sum_{l=i}^{i+k} n_l^Y \leq \sum_{j=i-\Delta}^{i+k+\Delta} n_j^X , \tag{1}$$

where $k = 0, 1, \ldots$ and n_j^X, n_l^Y are particle numbers in cells j, l of X and Y microstates, respectively. If the (anti)particle number in a single cell is unlimited, the inequalities concern bosons; if the number is limited to 0 and 1, they concern fermions.

Concerning quantum mechanics, the Cell Model for indistinguishable particles mimics the time evolution of a coherent quantum state of particles on a one-dimensional space lattice. Not considering particles' momenta and initially allowing all transitions corresponds to the (anti)particles' wave functions delocalising throughout the system. The Heisenberg uncertainty principle provides a simple and intuitive lower bound on momentum, which relates directly to quantum de-localisation and coherence: $\Delta p \approx \hbar/(2L)$, where L is the system size. The time steps correspond to the intervals between measurements of (anti)particle positions. Out of all possible transitions, the transport-locality condition (1) allows for only those that obey the speed-of-light limit. This, together with particle–antiparticle creation and annihilation, provides the model with the basic properties of quantum mechanics and relativistic physics.

Apparent teleportation within Cell Model is illustrated in Fig. 1. An example of the system's time evolution with $V = 9$ cells and periodic boundary conditions is shown. Cells contain "background" particles that carry total energy, depicted by the grey band. Particles and antiparticles of interest are depicted by red and blue circles, respectively. For simplicity, we assume that the speed-of-light limit implies $\Delta = 1$. The difference between the total number of particles and antiparticles is assumed to be conserved.

The case of indistinguishable particles and antiparticles is presented in plot (a) of Fig. 1. We postulate that only one particle exists at $t = 0$, and it is in cell 3. Three pairs of particles and antiparticles appear in cells 4, 5, and 6 at $t = 1$. At $t = 2$, the particle number distribution is shifted by one cell to the right by the transport-local transition. This is allowed by the transport-locality inequalities (1). Then, at $t = 3$, particle–antiparticle pairs annihilate, leaving a single particle in cell seven.

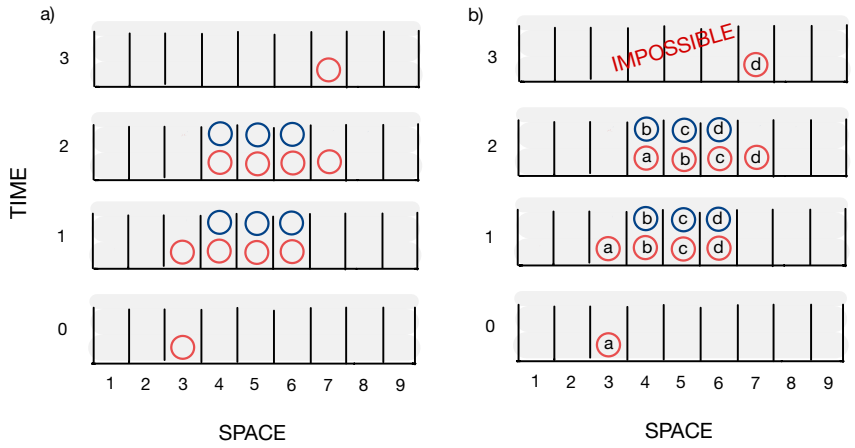

Fig. 1. The simple setup illustrates the apparent teleportation of indistinguishable particles within the Cell Model. The maximum distance a distinguishable particle and antiparticle can move during a time step is set to $\Delta = 1$. Three types of transitions — pair creation, local transport, and pair annihilation — are possible. (a) The example process with indistinguishable particles starting from a single particle in cell three at $t = 0$ and ending in a single particle in cell seven at $t = 3$. (b) Unsuccessful attempt to mimic the process by distinguishable particles. Three pairs of particles and antiparticles with identical labels appear at $t = 1$. Particles are shifted by one cell to the right at $t = 2$. In particular, particle "d" appears in cell seven. The particle number distributions for indistinguishable and distinguishable particles are identical at $t = 0$, 1, and 2. The pair annihilation reactions in cells 4, 5, and 6 are impossible during the third step because cells contain particles and antiparticles with different labels. For example, cell 4 contains particle "a" and antiparticle "b" at $t = 2$. See the text for more details.

Plot (b) of Fig. 1 shows an unsuccessful attempt to mimic the above process using distinguishable particles. In the example presented here, they are labelled by the letters "a", "b", "c", and "d". Similarly, antiparticles have unique labels. Only creating a particle and an antiparticle with identical labels is possible. Similarly, only a particle and an antiparticle with identical labels can annihilate.

For the label-blind observer, the particle and antiparticle number distributions of indistinguishable and distinguishable particles are identical at $t = 0, 1$, and 2. But the similarity breaks at $t = 3$. This is because annihilating particles and antiparticles with different labels is impossible. Of course, distinguishable particles can mimic the process depicted in plot (a) if the transport-locality requirement is lifted. Particle "a" can be "teleported" by four cells in three steps from cell 3 to 7.

The example construction of the process shown in Fig. 1 can be easily generalised, allowing for an arbitrary redistribution of indistinguishable boson-like particles and antiparticles in three time steps. This includes apparent teleportations — the processes which seemingly violate the speed-of-light limit.

We note that the microscopic mechanism of the apparent teleportation illustrated in Fig. 1 (a) cannot be used for superluminal signalling. An observer in cell seven detecting the particle at $t = 3$ cannot be sure it is caused by injecting a particle at $t = 0$ in cell three. For example, this can occur when a particle and an antiparticle pair are created in cell six independently of events in cell three. Then a particle appears in cell seven.

The probability of a given process depends on the dynamics, which in the Cell Model is encapsulated within the transition matrix. One can speculate that at sufficiently high-energy densities, the transition matrix of indistinguishable particles approaches maximum symmetry (the microstate symmetry [12]), and all processes have the same probability. This would imply that the system is "born in equilibrium" [13] — the probability of any microstate appearing at any time is equal. This may explain the puzzle of fast equilibration in heavy-ion collisions at high energies [14]. The apparent teleportation also may explain the quark–gluon paradox formulated in Ref. [15]. The transition of a large volume of quark–gluon plasma created in collisions of two atomic nuclei (see below for details) to colourless hadrons appears to require superluminal transport of colour charge to ensure local colour neutrality. Quarks and gluons are indistinguishable particles. Thus, the apparent teleportation may also provide an explanation for the quark–gluon plasma paradox.

The above discussion motivates the question of whether the apparent teleportation, if it exists, can be observed experimentally. This question is addressed in the following subsection.

2.2. Observing apparent teleportation

System of quarks and gluons created in nucleus–nucleus collisions at high energies is the highest energy density system ($\epsilon > 1$ GeV/fm^3 $\approx 1.6 \times 10^{35}$ J/m^3) created under conditions controlled in the laboratory [16]. Its equilibrium state is called quark–gluon plasma (QGP) [17]. The plasma expands and cools down, and the transition to colour-neutral hadrons — small bags of quarks and gluons — occurs at the hadronisation (transition) temperature $T_{\mathrm{HAD}} \approx 150$ MeV [18].

Six types of quarks (fermions) u, d, s, c, t, and b, and the corresponding antiquarks, and the eight types of gluons (bosons) can be created during the collision. Massless gluons and light u and d quarks and antiquarks are the

most abundant. Production of heavier quarks is suppressed even at the top collision energies of the CERN LHC [19]. The threshold for QGP creation in heavy-ion collisions is located at $\sqrt{s_{NN}} \approx 10$ GeV [20, 21]. For a review, see also Refs. [22, 23]. The fixed-target experiments at the CERN SPS measure heavy-ion collisions in the energy range $\sqrt{s_{NN}} \approx 5$–20 GeV. At the top of SPS energy, just above the QGP threshold energy, the mean number of light quarks and gluons produced in central collisions of two lead nuclei is of the order of 1000 [24]. The corresponding numbers for strange and charm quarks are ≈ 100 [24] and ≈ 1 [25], respectively.

The local creation and annihilation of c and $\bar{c}$ pairs implies that the energy and momentum scale of the interaction determines the c and $\bar{c}$ space-time separation via the uncertainty principle. The scale ranges between:

— the hard-scattering scale of the isolated reaction, $\hbar c/(2m_c) \approx 0.1$ fm, with $m_c \approx 1.3$ GeV being the charm-quark mass, and

— the thermal scale of the reaction in the dense quark–gluon plasma, $\hbar c/T \approx 1$ fm, with $T \approx 0.2$ GeV being the quark–gluon plasma temperature just above the transition (hadronisation) temperature.

The spatial extent and lifetime of the system created in central Pb+Pb collisions are of the order of approximately 10 fm, the diameter of the lead nucleus. It is much larger than the space-time cell in which local creation and annihilation of c and $\bar{c}$ quarks occur. It opens the possibility of observing the apparent teleportation in the collisions.

Observing apparent teleportation in heavy-ion collisions is likely to be a challenging task. This is due to two reasons:

— The experimental challenge: We cannot measure the location in the space of a single charm quark created in a collision at two different times. Hence, the simple setup presented in Fig. 1 cannot be used for observing the apparent teleportation.

— The theoretical challenge: Quantum Chromodynamics, the theory of strong interactions, does not provide quantitative predictions for multi-particle correlations in heavy-ion collisions; for further discussion, see Ref. [26].

However, with the help of well-established heavy-ion models, it may be possible to provide experimental evidence of the apparent teleportation by measuring momentum correlations between c and $\bar{c}$ quarks. The idea is rooted in our previous paper [26], which suggests the use of momentum correlations of charm–anticharm hadrons to extract information on spatial correlations of c and $\bar{c}$ quarks at hadronisation. The paper reviews experimental results on

charm–hadron correlations and collective flow. It also discusses the importance of having collisions with no more than one $c\bar{c}$ pair created. We note that the requirement of a single $c\bar{c}$ pair in a collision can be reconciled with the toy mechanism of the apparent teleportation presented in Section 2.1, assuming the coherent creation and annihilation of $c\bar{c}$ pairs in a short-time interval.

The standard model of heavy-ion collisions at high energies describes the collision as follows:

a. Initial stage: a high-density quark–gluon plasma is created. Theoretical approaches addressing this stage are discussed in Ref. [14].

b. Expansion stage: the plasma expands [27], cooling down to the hadronisation temperature ($T_{\mathrm{HAD}} \approx 150$ MeV in the local frame of the flowing matter). This stage is modelled using relativistic hydrodynamics [16].

c. Hadronisation stage: the plasma is converted into hadrons and resonances following statistical rules [28, 29] applied in the rest frame of a plasma fluid element. As a result, hadron momenta are determined by their flow acquired during the expansion stage and by the hadronisation (a local statistical process).

d. Free-streaming stage: resonances decay, and non-interacting hadrons freely stream in a vacuum to a detector.

We illustrate the idea of observing the apparent teleportation with the help of the schematic 1+1D model of the collisions sketched in Fig. 2. For simplicity, we assume that the initial stage is created at $t = 0$ and extends over the interval $-R$ to R. The hadronisation occurs at $t = R$; at this stage, the system extends from $-2R$ to $2R$. We also neglect the finite size of the space-time cell of the local $c\bar{c}$ pair creation. In plots (b) and (c), two examples of the hadronisation points of a single $c\bar{c}$ pair created in the collision are depicted as r_c and $r_{\bar{c}}$. The plots also show the past-light cones of the charm and anticharm quarks (represented by the blue and red areas).

Let us assume the c and $\bar{c}$ quarks were created in the same space-time point within the collision light cone and moved to hadronisation as distinguishable particles with subluminal velocities. In this case, the creation point has to be located inside the overlap between the collision light cone and the past-light cones of c and $\bar{c}$ quarks — the local-distinguishable (LD) condition. The $c\bar{c}$ pair depicted in Fig. 2 (b) fulfils the requirement, but the pair depicted in plot (c) does not. The latter implies that the process was not local-distinguishable, and one needs the apparent teleportation to explain it.

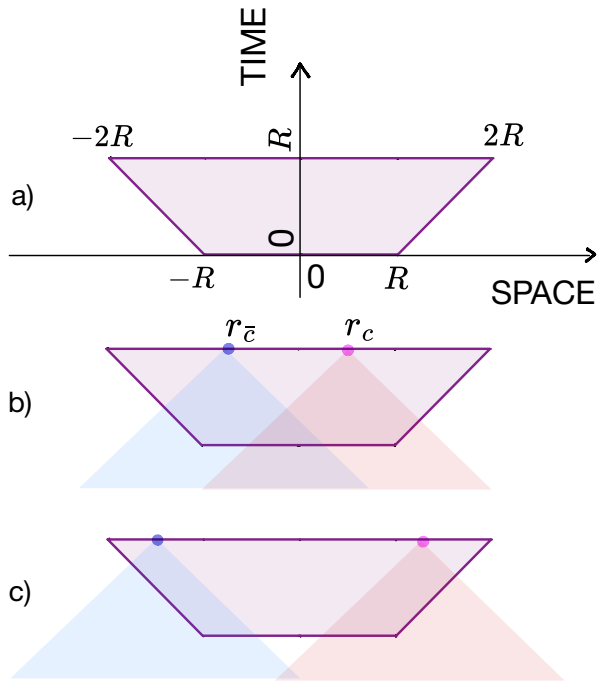

Fig. 2. The simplest illustration of observing the apparent teleportation in heavy-ion collisions at high energies using a single pair of c and $\bar{c}$ quarks. Plot (a) shows the space-time (1+1D) evolution of the quark–gluon plasma created at $t = 0$ in the spatial region from $-R$ to R. Hadronisation is assumed to occur at $t = R$, with the system extending from $-2R$ to $2R$. Plot (b) shows an example of the positions of the c and $\bar{c}$ quarks at hadronisation, denoted as r_c and $r_{\bar{c}}$, respectively. In this example, the past-light cones of the quarks overlap within the collision light cone. This overlap is required for the subluminal movement of distinguishable c and $\bar{c}$ quarks created at a common space-time point. We refer to this as the local-distinguishable condition. Plot (c) depicts the positions of the c and $\bar{c}$ quarks, which do not obey the condition and can only be explained by the apparent teleportation.

Within the example shown in Fig. 2, the LD condition reads $|r_c - r_{\bar{c}}| \leq 2R$. The apparent teleportation is required if the LD condition is violated, $|r_c - r_{\bar{c}}| > 2R$. The positions of quarks at hadronisation are not measured. Instead, experiments measure velocities (momenta) of charm hadrons in the free-streaming stage. We relate them in two steps: first, we introduce the correlation between the quark position and its flow velocity; second, we unfold the flow-velocity smearing arising from quark interactions with the medium and hadronisation.

Let us assume that the velocities of charm quarks at hadronisation are equal to the flow velocities of matter at the hadronisation points. For simplicity, we also assume that the flow velocity is proportional to the distance from the collision centre. From these assumptions, it follows that the apparent teleportation is required if $|\beta_c - \beta_{\bar{c}}| > 1$, where β_c and $\beta_{\bar{c}}$ are c and $\bar{c}$ quark velocities scaled by the light velocity. The pairs that obey the complementary condition, $|\beta_c - \beta_{\bar{c}}| \leq 1$, may come either from LD or AT processes. Allowed processes leading to pairs with given β_c and $\beta_{\bar{c}}$ values are depicted in Fig. 3.

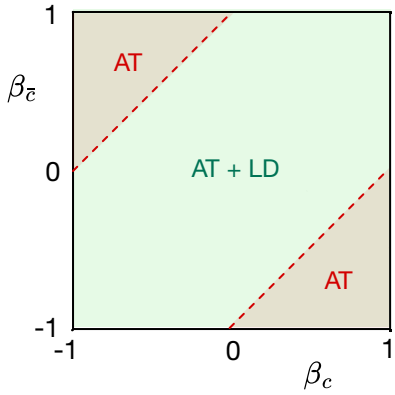

Fig. 3. The simplest 1+1D model of heavy-ion collisions and charm production explains the concept of observing apparent teleportation. Processes resulting in c and $\bar{c}$ quarks at hadronisation with flow velocities β_c and $\beta_{\bar{c}}$ are depicted as AT — apparent teleportation and LD — local distinguishable. The corners cut by the red dashed lines are forbidden for local distinguishable but allowed for the apparent teleportation processes.

After the hadronisation stage, the carriers of the c and $\bar{c}$ quarks are charm and anticharm hadrons. For simplicity, we assume these are D and $\bar{D}$ mesons. The free-streaming velocities of these mesons, β_D and $\beta_{\bar{D}}$, are superpositions of the quark flow velocities (β_c, $\beta_{\bar{c}}$) and a stochastic, non-flow component. The non-flow component may arise from initial momenta of quarks, their diffusion in quark–gluon plasma, hadronisation, and the following decay of resonances. In Methods A, we present a didactic illustration of the effect of the smearing of the flow components by the stochastic uncorrelated processes. We present results obtained within the schematic 1+1D model with Hubble-like initial and hadronisation hypersurfaces.

Finally, in Methods B, the 1+3D model of high-energy nucleus–nucleus collisions, with properties that enable predictions of experimentally measured quantities, is presented. It utilises the Blast-Wave model [30] of radial flow. The results indicate that the distribution of the opening angle be-

tween momenta of D and $\bar{D}$ mesons may yield evidence for the apparent teleportation. Assuming that the stochastic components of D and $\bar{D}$ are uncorrelated, this distribution can be corrected for the smearing in an almost model-independent manner. The procedure is detailed in Ref. [26].

The initial c and $\bar{c}$ momenta may be correlated due to energy-momentum conservation. Remnants of this correlation might persist throughout the transport process, leading to correlated non-flow components in the D and $\bar{D}$ momenta. At collision energies where the creation of c and $\bar{c}$ quarks occurs near the threshold — such that no more than one $c\bar{c}$ pair is produced per collision — it is reasonable to expect that the initial quark momenta are small. Consequently, the correlated non-flow component is likely negligible. A quantitative estimate of this effect lies beyond the scope of the present paper.

The apparent teleportation may render all transitions possible. One may speculate that at very high energy densities, the microstate-symmetric transition matrix [12] may govern the system's evolution. This implies that c and $\bar{c}$ quarks, and consequently D and $\bar{D}$ hadrons, are produced independently in space-time and momentum. The joint probability density function $\rho(\beta_D, \beta_{\bar{D}})$ factorises as

$$\rho(\beta_D, \beta_{\bar{D}}) = \rho(\beta_D) \cdot \rho(\beta_{\bar{D}}) \,, \tag{2}$$

and, in the general 1+3D case,

$$\rho(\boldsymbol{p}_D, \boldsymbol{p}_{\bar{D}}) = \rho(\boldsymbol{p}_D) \cdot \rho(\boldsymbol{p}_{\bar{D}}) \,, \tag{3}$$

where $\boldsymbol{p}_D$ and $\boldsymbol{p}_{\bar{D}}$ are the momentum vectors of D and $\bar{D}$ hadrons, respectively. Contemporary experiments can soon test this extreme prediction under the apparent teleportation hypothesis [26]. This requires measurements of sufficiently high statistics of charm and anticharm hadron pairs produced in individual collisions with a mean multiplicity of pairs below one [26].

3. Discussion

We argue that the apparent teleportation of indistinguishable particles naturally follows from the Standard Model postulate of elementary particles being indistinguishable. Thus, apparent teleportation is expected in many systems of indistinguishable particles and antiparticles.

The presented toy-model example of the apparent teleportation mechanism suggests that the coherent creation and annihilation of particle–antiparticle pairs is required for apparent teleportation. Thus, apparent teleportation is expected to be more popular in high-energy-density systems. It makes it difficult to observe experimentally. This is because the high-density

systems created in laboratories typically have small spatial and temporal dimensions. Therefore, precisely measuring particle number distribution in short-time intervals may be challenging.

We provide an example of how to overcome the problem of observing apparent teleportation. It can be done by measuring the momentum correlation of charm and anticharm hadrons produced in collisions of two sufficiently heavy atomic nuclei, with only one pair of charm and anticharm quarks created. Contemporary experiments can perform the measurement; however, interpreting the results in terms of apparent teleportation will depend on modelling the time evolution of the strongly interacting system.

To strengthen the conclusions regarding apparent teleportation, additional experimental setups should be considered. The example presented above concerns apparent teleportation driven by strong interactions. It can be straightforwardly extended from the charm–anticharm hadron correlations to the bottom–antibottom hadron correlations. The mean number of b and $\bar{b}$ pairs, $\langle b\bar{b}\rangle$, produced in central Pb+Pb collisions at the top LHC energy is expected to be of the order of 10 [31]. Thus, by lowering the LHC beam energy, the condition $\langle b\bar{b}\rangle \approx 1$ can be reached. Alternatively, one can consider the possibility of the measurements at the top RHIC energy by the operational sPHENIX experiment [32]. The corresponding measurements of bottom–antibottom hadron correlations may be challenging due to the low detection probability in central Pb+Pb collisions recorded in collider mode.

The possibility of using strange–antistrange hadron correlations to search for the apparent teleportation should also be considered. The requirement of a mean number of strange and antistrange hadrons being of the order of one implies measuring their correlations in central Pb+Pb collisions at collision energies of several GeV [33]. These are energies of the future CBM experiment at FAIR [34]. They are below the onset of the quark–gluon plasma creation [20, 21]. Thus, the carriers of strangeness are different species of strange and antistrange hadrons and resonances. This brings the system closer to the system of distinguishable particles for which, by definition, the apparent teleportation does not exist. Thus, one expects that at energies below the onset of quark–gluon plasma creation, the chance to observe the apparent teleportation is reduced. This concerns the search for the apparent teleportation via correlations of strange–antistrange hadrons.

Finally, we consider the possibility of observing apparent teleportation driven by electromagnetic interactions. It seems that the simplest setup consists of an extended system of photons at energy density close to the Schwinger limit for spontaneous creation of e^+–e^- pairs [35]. In terms of the electric field strength, the Schwinger limit is about 1.3×10^{18} V/m, which corresponds to the energy density $\approx 10^{18}$ J/m^3 ($\approx 10^6$ GeV/fm^3). Existing and planned ultra-intense laser facilities, like the Extreme Light Infrastructure in Europe, are far below the Schwinger limit.

Ultra-peripheral heavy-ion collisions (UPCs) at the LHC may provide an opportunity to search for apparent teleportation driven by electromagnetic interactions. In such collisions, a photon interacts with a strong electromagnetic field created by a heavy ion moving with ultra-relativistic velocities. These conditions facilitate the production of $c\bar{c}$ pairs; see, for example, measurements of charmonium production in the UPCs by the LHC experiments [36–38] or a recent report on D^0 production in UPCs by the CMS experiment [39]. Thus, in principle, a measurement of D–$\bar{D}$ correlation is possible, simultaneously fulfilling the requirement of a single charm pair created in a collision. However, the probability of apparent teleportation is likely significantly lower under these conditions, and a feasibility study is necessary to determine an optimal experimental setup for its observation. Other probes (strangeness, e^+–e^- pairs) could also be considered.

If it exists, the apparent teleportation may explain two puzzles of strong interactions at high-energy densities: the rapid equilibration of the created system of quarks and gluons, and its rapid hadronisation, both of which satisfy the requirement of local colour neutrality.

We thank F. Giacosa, M. Gorenstein, D. Miskowiec, and St. Mrowczynski for their comments. This work is partially supported by the National Science Centre (NCN), Poland, grants 2018/30/A/ST2/00226, 2018/30/E/ST2/00089, and 2020/39/D/ST2/02054.

Data availability statement

The data that support the findings of this study are available from the corresponding author upon reasonable request.

Code availability

The software used for the studies presented in this paper is available from the corresponding author upon reasonable request.

Appendix A

The 1+1D Hubble-like model

Here, we illustrate the effect of smearing due to stochastic, uncorrelated processes, taking as an example the statistical hadronisation of charm and anticharm quarks. We present the results obtained within the schematic 1+1D model with the Hubble-like initial and hadronisation hypersurfaces.

The shape of the initial system is described by its initial hypersurface

$$t^2 = z^2 + \tau_0^2\,, \tag{A.1}$$

where τ_0 is the initial proper time the system is formed, and z is the distance from the system's centre. The system then undergoes a Hubble-like expansion, and the hadronisation hypersurface is taken as

$$t^2 = z^2 + \tau_{\mathrm{HAD}}^2 \,, \tag{A.2}$$

where τ_{HAD} is the hadronisation proper time. The expanding matter is assumed to be in local equilibrium corresponding to temperatures T_0 and T_{HAD} at proper times τ_0 and τ_{HAD}, respectively. The matter density is assumed to be uniform along the hadronisation hypersurface, which is limited in z as $|z| < \tau_{\mathrm{HAD}} + R_{\mathrm{MAX}}$. In the following, the parameters τ_{HAD} and R_{MAX} are fixed to 10 fm and 6 fm, being of the order of the Pb nucleus radius. Figure 4 shows a sketch illustrating the hypersurfaces and indicating their parameters.

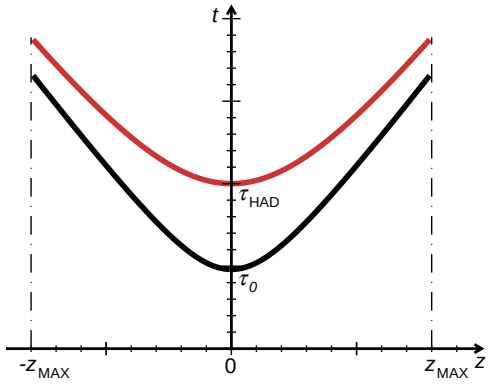

Fig. 4. Sketch of the 1+1D Hubble-like model of the space-time evolution of the system created in lead–lead collisions. The black curve shows the initial hypersurface defined by the proper time τ_0 at which the system is formed, and its expansion starts. The red curve presents the hadronisation hypersurface given by the τ_{HAD} parameter.

For the Hubble-like flow, the energy conservation relates the initial parameters τ_0 and T_0 to the hadronisation parameters τ_{HAD} and T_{HAD} as

$$\frac{\tau_0}{\tau_{\mathrm{HAD}}} = 1 - \frac{3}{4} \ln\left(\frac{T_0}{T_{\mathrm{HAD}}}\right) . \tag{A.3}$$

The hadronisation temperature is set to the well-known value from the lattice QCD, $T_{\mathrm{HAD}} = 150$ MeV [18]. The initial temperature T_0 must exceed the hadronisation temperature. Below, we present examples calculated for $T_0 = 200$ MeV and $T_0 = 300$ MeV. The latter value is close to the initial temperature given by the Fermi–Landau initial conditions [24] at the top energy of the CERN SPS. It can be considered as the upper limit of T_0 at SPS.

The remaining parameter of the model τ_0 is calculated using Eq. (A.3). The velocity of the fluid element and (anti)charm quarks at the hadronisation is given by the Hubble flow assumption, $u = z/\tau_{\mathrm{HAD}}$.

At hadronisation, (anti)charm quarks are converted into (anti) D mesons. To model this process, the momentum of the (anti)charmed mesons at the fluid rest frame p'_D is drawn from the statistical-like distribution

$$dN/dp'_D \quad \propto \quad {p'_D}^2 \cdot e^{-\sqrt{m_D^2+{p'_D}^2} \;/\; T_{\mathrm{HAD}}}, \tag{A.4}$$

where we use the mass of D^0 meson $m_D = 1.869$ GeV. Finally, the momentum p_D in the laboratory frame at hadronisation is calculated by boosting p'_D with the fluid-element velocity. To assess how the statistical hadronisation influences the expected signal of the apparent teleportation, we also considered a case with $p'_D = 0$, thus removing the effect of statistical smearing of the momentum of (anti)charm mesons.

Figure 5 shows two examples ($T_0 = 200$ MeV (a) and $T_0 = 300$ MeV (b)) of the hadronisation points of charm and anticharm quarks requiring the apparent teleportation — the past-light cones of c and $\bar{c}$ quarks overlap only below the initial hypersurface. We observe that the larger T_0 is, the smaller the space for separating apparent teleportation from local distinguishable processes. The apparent teleportation processes can be separated up to $T_0 \approx 400$ MeV within the model, with its other parameters set to the values given in the text.

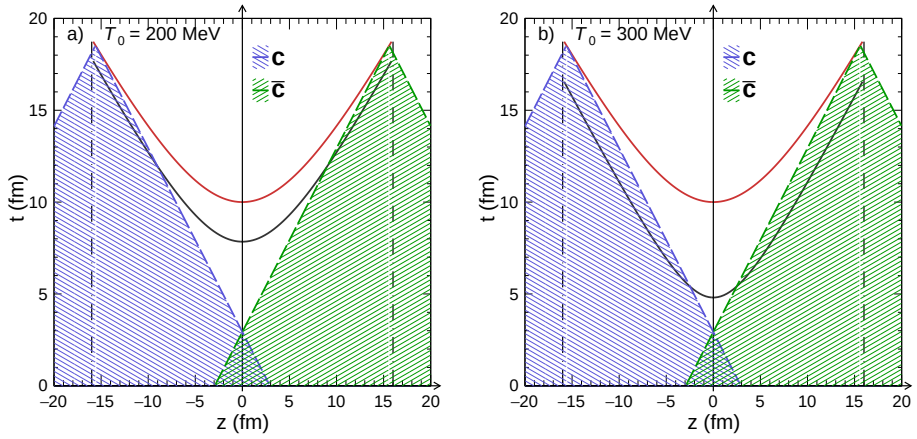

Fig. 5. Examples of hadronisation points of c and $\bar{c}$ quarks that can only result from the apparent hadronisation. The initial temperature is set to $T_0 = 200$ MeV (a) and $T_0 = 300$ MeV (b). The black lines indicate the initial hypersurface, and the hadronisation hypersurface is shown by red lines.

Figures 6 and 7 show the joint rapidity ($y = \tanh^{-1}(\beta)$) distributions of D and $\bar{D}$ mesons for $\tau_{\mathrm{HAD}} = 10$ fm for $T_0 = 200$ MeV and $T_0 = 300$ MeV, respectively. The space for separating the apparent teleportation is significantly larger for the lower value of T_0. Including statistical hadronisation significantly smears the joint rapidity distributions.

Our study shows that apparent teleportation can be observed in heavy-ion collisions at the SPS energy. The chance of success depends on the system's initial temperature and the hadronisation hypersurface.

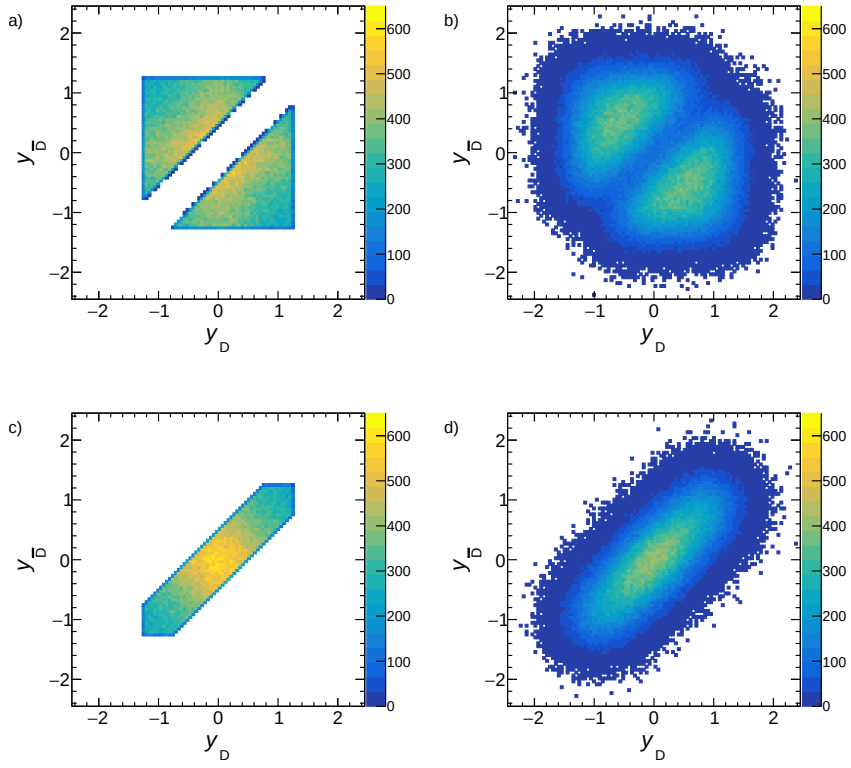

Fig. 6. Joint rapidity distributions of D and $\bar{D}$ mesons for the initial temperature $T_0 = 200$ MeV. Plots (a) and (b) show the distributions for D and $\bar{D}$ pairs, which can result only from the apparent teleportation. Plots (c) and (d) show the results for the pairs, which can be attributed either to local-distinguishable processes or the apparent teleportation. Plots (a) and (c) are obtained without smearing due to statistical hadronisation, whereas plots (b) and (d) include the smearing.

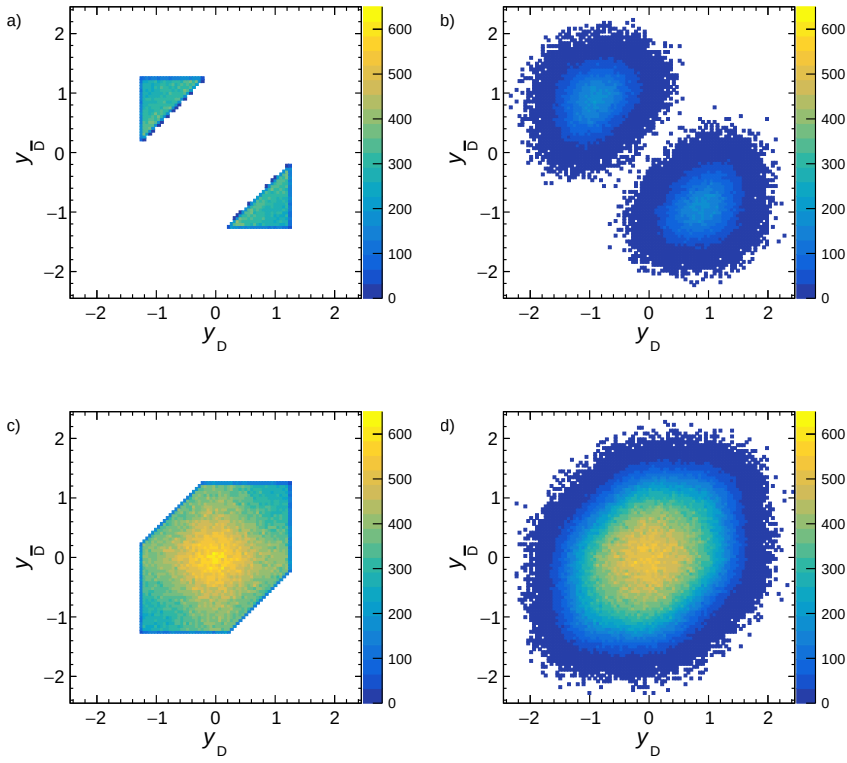

Fig. 7. Joint rapidity distributions of D and $\bar{D}$ mesons for the initial temperature $T_0 = 300$ MeV. Plots (a) and (b) show the distributions for D and $\bar{D}$ pairs, which can result only from the apparent teleportation. Plots (c) and (d) show the results for the pairs, which can be attributed either to local-distinguishable processes or the apparent teleportation. Plots (a) and (c) were obtained without smearing due to statistical hadronisation, whereas plots (b) and (d) include the smearing.

Appendix B

The 1+3D Blast-Wave model

The 1+3D model of high-energy nucleus–nucleus collisions, with properties that enable the prediction of experimentally measured quantities required to observe the apparent teleportation, is presented here. The model utilises the Blast-Wave model [30] of radial flow, which has been widely used for parametrising experimental results on hadron spectra for decades. Here, only central Pb+Pb collisions are considered.

The model assumptions are as follows:

(i) The initial stage ($t = 0$) of the matter created in a central Pb+Pb collision is approximated as a sphere of radius $R = 6$ fm (the radius of the Pb nucleus), centred at the origin of the coordinate system. The density is assumed to be isotropic.

(ii) The hadronisation stage, where the radial flow stops, is approximated as a sphere with radius $2R$.

(iii) The radial flow velocity at hadronisation at position $\boldsymbol{r} = (x, y, z)$ is given by

$$\boldsymbol{v}(\boldsymbol{r}) = c \cdot \boldsymbol{r}/(2R)\,, \tag{B.1}$$

where c is set to one. The hadronistation occurs at time $t_{\mathrm{HAD}} = R/v(r = 2R) = c/R$.

The distribution function of a pair of D and $\bar{D}$ mesons generally depends on six momentum components ($\boldsymbol{p}_D$ and $\boldsymbol{p}_{\bar{D}}$). However, due to the model's spherical symmetry, this dependence reduces to three non-trivial momentum quantities. Here, we select them as:

— The opening angle between the momentum vectors, Θ, where $\Theta = |\theta_D - \theta_{\bar{D}}|$ and θ_D, $\theta_{\bar{D}}$ are the polar angles of D, $\bar{D}$ mesons changing in the range $[0, \pi]$.

— The momentum magnitudes p_D and $p_{\bar{D}}$.

The model predictions are as follows.

Neglecting the non-flow component of the final velocity, if the hadronisation points of c and $\bar{c}$ are chosen independently, the cosine of the opening angle, $\cos(\Theta)$, is uniformly distributed. This set of pairs includes both local-distinguishable pairs and those violating this condition.

At $t = 0$, the collision light cone is a sphere with radius R centred at $(0, 0, 0)$. The past-light cones of the hadronising c and $\bar{c}$ quarks on a sphere with radius $r = aR$ ($0 \le a \le 2$) are also spheres of radius R, but centred at $\boldsymbol{r}_c$ and $\boldsymbol{r}_{\bar{c}}$ ($r_c = r_{\bar{c}} = aR$), respectively.

The maximum allowed opening angle $\Theta_{\mathrm{MAX}}(aR)$ for which the LD condition is obeyed is

$$\Theta_{\mathrm{MAX}}(aR) = \pi - \cos^{-1}\left(1 - a^2/2\right)\,. \tag{B.2}$$

For $a = 2$ (the maximum hadronisation surface radius), $\Theta_{\mathrm{MAX}} = 0$, while for $a \to 1$, $\Theta_{\mathrm{MAX}} \to 2/3\ \pi$. For $a = 1$ and below, $\Theta_{\mathrm{MAX}} = \pi$. A sketch illustrating this calculation is shown in Fig. 8.

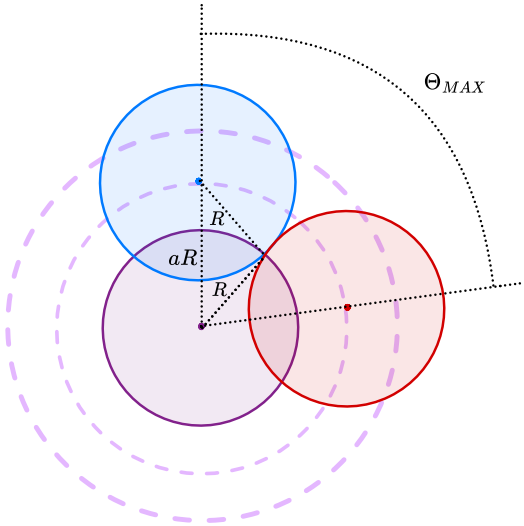

Fig. 8. Sketch illustrating the calculation of the maximum possible opening angle Θ_{MAX} between the c and $\bar{c}$ quarks hadronising at $r = a \cdot R$ and obeying the LD condition. The plot shows the intersection of the plane defined by the hadronisation points and the collision centre with the past-light-cone spheres of the c (red) and $\bar{c}$ quarks, as well as the collision light cone at $t = 0$. The angle Θ_{MAX} is determined by the requirement of a single common point of the three circles.

The LD condition suppresses the opening angle distribution at large angles, with the effect strongest for pairs emitted from $r = 2R$, where $\Theta_{\mathrm{MAX}} = 0°$. For pairs hadronising at small radii ($r \leq R$), one gets $\Theta_{\mathrm{MAX}} = \pi$.

One can focus on pairs emitted from the outer hadronisation layer (high momentum) to test for apparent teleportation. Observing pairs with $\Theta > \Theta_{\mathrm{MAX}}$ at high momentum would indicate apparent teleportation of c and $\bar{c}$ quarks.

Various processes, in particular, hadronisation of (anti)charm quarks, will smear the opening angle distribution between D and $\bar{D}$ mesons. Thus, separating the apparent teleportation will require correcting the opening angle distribution for the smearing as discussed in Ref. [26]. As the smearing will be mostly due to effects that affect the emission angles of D and $\bar{D}$ independently, the correction is expected to be approximately model-independent.

REFERENCES

[1] M. Maku, «Teleportation and Science Fiction», *Random House Digital*, 2008.

[2] C.H. Bennett *et al.*, «Teleporting an unknown quantum state via dual classical and Einstein–Podolsky–Rosen channels», *Phys. Rev. Lett.* **70**, 1895 (1993).

[3] D. Bouwmeester *et al.*, «Experimental quantum teleportation», *Nature* **390**, 575 (1997).

[4] J. Yin *et al.*, «Satellite-based entanglement distribution over 1200 kilometers», *Science* **356**, aan3211 (2017).

[5] W. Pfaff *et al.*, «Unconditional quantum teleportation between distant solid-state quantum bits», *Science* **345**, 532 (2014).

[6] S. Pirandola *et al.*, «Advances in quantum teleportation», *Nature Photon* **9**, 641 (2015).

[7] M.A. Porras, M. Casado-Álvaro, I. Gonzalo, «Teleportation of a quantum particle in a potential via quantum Zeno dynamics», *Phys. Rev. A* **109**, 032207 (2024).

[8] P. Facchi *et al.*, «Quantum Zeno dynamics», *Phys. Lett. A* **275**, 12 (2000).

[9] P. Facchi, S. Pascazio, «Quantum Zeno Subspaces», *Phys. Rev. Lett.* **89**, 080401 (2002).

[10] P. Facchi, S. Pascazio, «Quantum Zeno dynamics: mathematical and physical aspects», *J. Phys. A: Math. Theor.* **41**, 493001 (2008).

[11] M. Gazdzicki *et al.*, «Steady state of isolated systems *versus* microcanonical ensemble in cell model of particle creation and annihilation», *Int. J. Mod. Phys. E* **26**, 1750085 (2017).

[12] M. Gazdzicki *et al.*, «Equilibration and Locality», *Acta Phys. Pol. B* **53**, 8-A2 (2022).

[13] R. Hagedorn, «Statistical thermodynamics of strong interactions at high-energies», *Nuovo Cim. Suppl.* **3**, 147 (1965).

[14] S. Schlichting, D. Teaney, «The First fm/c of Heavy-Ion Collisions», *Annu. Rev. Nucl. Part. Sci.* **69**, 447 (2019).

[15] D. Miśkowiec, «Quark–gluon plasma paradox», *PoS* **(CPOD07)**, 020 (2007).

[16] W. Florkowski, «Phenomenology of Ultra-relativistic Heavy-ion Collisions», *World Scientific*, 2010.

[17] E.V. Shuryak, «Quantum chromodynamics and the theory of superdense matter», *Phys. Rep.* **61**, 71 (1980).

[18] Y. Aoki, Z. Fodor, S.D. Katz, K.K. Szabo, «The QCD transition temperature: Results with physical masses in the continuum limit», *Phys. Lett. B* **643**, 46 (2006).

[19] ALICE Collaboration (B. Abelev *et al.*), «Centrality dependence of π, K, and p production in Pb–Pb collisions at $\sqrt{s_{NN}} = 2.76$ TeV», *Phys. Rev. C* **88**, 044910 (2013).

[20] NA49 Collaboration (S.V. Afanasiev *et al.*), «Energy dependence of pion and kaon production in central Pb+Pb collisions», *Phys. Rev. C* **66**, 054902 (2002).

[21] NA49 Collaboration (C. Alt *et al.*), «Pion and kaon production in central Pb+Pb collisions at 20 A and 30 A GeV: Evidence for the onset of deconfinement», *Phys. Rev. C* **77**, 024903 (2008).

[22] M. Gazdzicki, M. Gorenstein, P. Seyboth, «Onset of Deconfinement in Nucleus–Nucleus Collisions: Review for Pedestrians and Experts», *Acta Phys. Pol. B* **42**, 307 (2011).

[23] E. Andronov, M. Kuich, M. Gaździcki, «Diagram of High-Energy Nuclear Collisions», *Universe* **9**, 106 (2023).

[24] M. Gazdzicki, M.I. Gorenstein, «On the Early Stage of Nucleus–Nucleus Collisions», *Acta Phys. Pol. B* **30**, 2705 (1999).

[25] NA61/SHINE Collaboration (A. Merzlaya), «First $D^0 + \bar{D}^0$ measurement in nucleus–nucleus collisions at SPS energies with NA61/SHINE», *EPJ Web Conf.* **316**, 04004 (2025).

[26] M. Gazdzicki, D. Kikoła, I. Pidhurskyi, L. Tinti, «Spatial correlations of charm and anticharm quarks at hadronisation», *Commun. Phys.* **8**, 304 (2025).

[27] L.D. Landau, «On the multiparticle production in high-energy collisions», *Izv. Akad. Nauk Ser. Fiz.* **17**, 51 (1953).

[28] R. Hagedorn, J. Rafelski, «Hot hadronic matter and nuclear collisions», *Phys. Lett. B* **97**, 136 (1980).

[29] F. Becattini, J. Manninen, M. Gazdzicki, «Energy and system size dependence of chemical freeze-out in relativistic nuclear collisions», *Phys. Rev. C* **73**, 044905 (2006).

[30] E. Schnedermann, J. Sollfrank, U.W. Heinz, «Thermal phenomenology of hadrons from 200 GeV S+S collisions», *Phys. Rev. C* **48**, 2462 (1993).

[31] M. He, R. Rapp, «Bottom Hadrochemistry in High-Energy Hadronic Collisions», *Phys. Rev. Lett.* **131**, 012301 (2023).

[32] sPHENIX Collaboration (Z. Shi), «Heavy Flavor Physics at the sPHENIX Experiment», *Universe* **10**, 126 (2024).

[33] C. Blume, C. Markert, «Strange hadron production in heavy ion collisions from SPS to RHIC», *Prog. Part. Nucl. Phys.* **66**, 834 (2011).

[34] CBM Collaboration (T. Ablyazimov *et al.*), «Challenges in QCD matter physics — The scientific programme of the Compressed Baryonic Matter experiment at FAIR», *Eur. Phys. J. A* **53**, 60 (2017).

[35] J.S. Schwinger, «On Gauge Invariance and Vacuum Polarization», *Phys. Rev.* **82**, 664 (1951).

[36] CMS Collaboration (A. Tumasyan *et al.*), «Probing Small Bjorken-x Nuclear Gluonic Structure via Coherent J/ψ Photoproduction in Ultraperipheral Pb–Pb Collisions at $\sqrt{s_{NN}} = 5.02$ TeV», *Phys. Rev. Lett.* **131**, 262301 (2023).

[37] ALICE Collaboration (S. Acharya *et al.*), «Coherent J/ψ and ψ' photoproduction at midrapidity in ultra-peripheral Pb–Pb collisions at $\sqrt{s_{NN}} = 5.02$ TeV», *Eur. Phys. J. C* **81**, 712 (2021).

[38] LHCb Collaboration (R. Aaij *et al.*), «Study of coherent J/ψ production in lead–lead collisions at $\sqrt{s_{NN}} = 5$ TeV», *J. High Energy Phys.* **2022**, 117 (2022).

[39] CMS Collaboration, Technical report, CERN, Geneva, 2024.